ORIGINAL RESEARCH

Physiologia Plantarum

Overexpression of the plastidial pseudo-protease AtFtsHi3 enhances drought tolerance while sustaining plant growth

Laxmi S. Mishra[1] | Sam D. Cook[1] | Sunita Kushwah[1] | Hanna Isaksson[2,3] |
Isabella R. Straub[4] | Miriam Abele[4] | Sanatkumar Mishra[5] | Christina Ludwig[4] |
Eric Libby[2,3] | Christiane Funk[1]

[1]Department of Chemistry, Umeå University, Umeå, Sweden

[2]Department of Mathematics and Mathematical Statistics, Integrated Science Lab (Icelab), Umeå University, Umeå, Sweden

[3]IceLab, Umeå University, Umeå, Sweden

[4]Bavarian Center for Biomolecular Mass Spectrometry (BayBioMS), School of Life Sciences Weihenstephan, Technical University of Munich (TUM), Freising, Germany

[5]Umeå Plant Science Centre, Department of Forest Genetics and Plant Physiology, Swedish University of Agricultural Sciences, Umeå, Sweden

Correspondence
Christiane Funk,
Email: christiane.funk@umu.se

Present addresses
Laxmi S. Mishra, Department of Plant Biology, Swedish University of Agricultural Sciences, Uppsala, Sweden; and Sanatkumar Mishra, Novavax AB, KLÖVERN Kungshörnet, Uppsala, Sweden.

Abstract

With climate change, droughts are expected to be more frequent and severe, severely impacting plant biomass and quality. Here, we show that overexpressing the Arabidopsis gene *AtFtsHi3* (*FtsHi3OE)* enhances drought-tolerant phenotypes without compromising plant growth. *AtFtsHi3* encodes a chloroplast envelope pseudo-protease; knock-down mutants (*ftshi3-1*) are found to be drought tolerant but exhibit stunted growth. Altered *AtFtsHi3* expression therefore leads to drought tolerance, while only diminished expression of this gene leads to growth retardation. To understand the underlying mechanisms of the enhanced drought tolerance, we compared the proteomes of *ftshi3-1* and *pFtsHi3-FtsHi3OE (pFtsHi3-OE)* to wild-type plants under well-watered and drought conditions. Drought-related processes like osmotic stress, water transport, and abscisic acid response were enriched in *pFtsHi3-OE* and *ftshi3-1* mutants following their enhanced drought response compared to wild-type. The knock-down mutant *ftshi3-1* showed an increased abundance of HSP90, HSP93, and TIC110 proteins, hinting at a potential downstream role of AtFtsHi3 in chloroplast pre-protein import. Mathematical modeling was performed to understand how variation in the transcript abundance of *AtFtsHi3* can, on the one hand, lead to drought tolerance in both overexpression and knock-down lines, yet, on the other hand, affect plant growth so differently. The results led us to hypothesize that AtFtsHi3 may form complexes with at least two other protease subunits, either as homo- or heteromeric structures. Enriched amounts of AtFtsH7/9, AtFtsH11, AtFtsH12, and AtFtsHi4 in *ftshi3-1* suggest a possible compensation mechanism for these proteases in the hexamer.

1 | INTRODUCTION

Drought is one of the most severe environmental stresses affecting plant biomass production and quality (Seleiman et al., 2021). Several classes of proteolytic enzymes are involved in the response to drought (Vaseva et al., 2011; Fanourakis et al., 2020). Despite progress in understanding the implication of the *FTSH* gene family in adaptation to drought stress, the underlying molecular mechanisms still need to be investigated.

FtsH proteases are membrane-bound zinc metalloproteases present in eubacteria, animals, and plants and play a critical role in the proteolysis of membrane proteins. Arabidopsis contains 12 members of the FtsH family (FtsH 1–12), which are localized in the organelles of endosymbiotic origin, the mitochondria and chloroplasts (Smakowska et al., 2014; Nishimura et al., 2016; Bittner et al., 2017). As ATP-dependent metalloproteases, FtsH proteases contain a recognized AAA+ domain (IPR003593), a region of approximately 250 amino acids positioned between the transmembrane helices and the proteolytic zinc-binding M41 peptidase domain (IPR000642) (Martin, 2021). Besides the proteolytically active FtsH proteases, pseudo-proteases, termed FtsHi, i for inactive (Sokolenko et al., 2002), have been identified in the genomes of plants. Five AtFtsHi enzymes are present in *Arabidopsis thaliana*, all localized in the chloroplast envelope. In these, the consensus sequence HEXXH of the Zn^+-binding M41 peptidase domain is either absent (AtFtsHi3) or altered (AtFtsHi1/2/4/5) (Wagner et al., 2012). *Ycf*2 (hypothetical chloroplast open reading frame 2) has been suggested to encode a sixth FtsHi enzyme in *Arabidopsis thaliana* (Kikuchi et al., 2018), which also occurs in the green alga *Chlamydomonas reinhardtii* (Ramundo et al., 2020). AtFtsHi1, 2, 4, 5 form an import motor complex with AtFtsH12, a NAD-dependent malate dehydrogenase (MDH) (Schreier et al., 2018, Mielke et al., 2020) and possibly Ycf2 (Kikuchi et al., 2018). Homozygous mutants lacking functional AtFtsHi1, 2, 4, or 5 also show a seed-lethal phenotype (Kadirjan-Kalbach et al., 2012; Lu et al., 2014; Wang et al., 2018; Mishra et al., 2019), whereas heterozygous *FtsHi* mutants and plants carrying point/missense or "*weak*" mutations display a pale-green-seedling phenotype. These plants have smaller rosettes throughout their life span (Kadirjan-Kalbach et al., 2012; Lu et al., 2014; Mishra et al., 2019; Mishra et al., 2021) and often contain variegated leaves (Wang et al., 2018). AtFtsHi3 was not identified as a component in the FtsH12/FtsHi1,2,4,5/MDH/Ycf2 complex (Kikuchi et al., 2018), and its interacting partners remain unknown. Also, homozygous *Atftshi3* mutants are not embryo-lethal (Kikuchi et al., 2018; Mishra et al., 2019; Mishra et al., 2021). A *Atftshi3-1* knockdown mutant, which has significantly reduced *AtFtsHi3* expression (termed *ftshi3-1* (kd) in Mishra et al., 2021), is drought tolerant. However, its growth is strongly affected, and seed germination is somewhat delayed.

Here, we show that overexpression of the *AtFtsHi3* gene results in a drought-tolerant phenotype. We demonstrate that overexpression of *AtFtsHi3* impacts leaf stomatal density, lowers stomatal conductance and increases the water use efficiency index (WUEi). The levels of several ABA-responsive genes in *pFtsHi3-OE* plants were elevated (relative to the wild type (WT)) in watered conditions, although their expression in drought did not change substantially in these lines. Comparing the proteomes of *ftshi3-1* and *pFtsHi3-OE* to WT revealed that several drought-associated processes are repressed in the mutants, such as response to water deprivation and response to abscisic acid (ABA). Mathematical modeling was performed to understand how variation in the transcript abundance of *AtFtsHi3* can, on the one hand, lead to drought tolerance in both overexpression and mutant lines, yet on the other hand, affect plant growth so differently. These models conclude that AtFtsHi3 may form complexes with at least two other protease subunits. The chloroplast envelope located AtFtsH7/9 and AtFtsH11, AtFtsH12 and AtFtsHi4 were detected in the proteomes of *ftshi3-1*, independent of the growth conditions but not in *pFtsHi3-OE* or WT. These enzymes, therefore, might be possible complex partners substituting for the lost subunit.

2 | MATERIALS AND METHODS

2.1 | Plant material and growth conditions

Arabidopsis wild type (WT) Columbia (col 0) ecotype and mutant seeds were sterilized with 10% NaCl, washed 4X with sterile water, and then stratified for two days at 4°C. The seeds were selected on full-strength MS (Murashige & Skoog) agar (Murashige and Skoog, 1962), supplemented with 1% sucrose and 75 µg l^{-1} sulfadiazine. After 12 days post-germination on plates, the plants were transferred to soil. Water-deficit stress was applied on plants grown on soil in a growth chamber under short-day conditions (8 /16 h photoperiod, 22/18°C), with a relative humidity of 50% and 150 µmol photons m^{-2} s^{-1} after approximately four weeks.

2.2 | Generation of transgenic Arabidopsis seedlings

To generate *AtFtsHi3* overexpression lines, a 2524-bp genomic region containing the full-length *AtFtsHi3* gene was amplified from *A. thaliana* by Phusion® proofreading polymerase (Thermo Fisher Scientific). To generate plants with an additional *FtsHi3* gene under its native promoter *pFtsHi3-OE* lines(*pFtsHi3-FtsHi3OE*), a construct containing the amplified *FtsHi3* promoter sequence, 1059 bp upstream of the *FtsHi3* ATG start codon was amplified by PCR (as predicted by Knudsen, 1999) using the primers 'ftshi3 Promoter Forward' and 'ftshi3 Reverse for HA-line' (Table S7). The PCR product containing the *pAtFtsHi3::FtsHi3* genomic DNA was cloned into a pENTR/D-TOPO vector and transferred into the destination vector pGWB15, resulting in a 3xHA-tagged gene product. To generate plants overexpressing *AtFtsHi3* under a 35S promoter (*35SFtsHi3-OE*) the coding sequence of *FtsHi3* was amplified and cloned into a pGWB5 vector under the control of the CaMV35S promoter; primers used are listed in (Table S7). The binary plasmids (*pAtFtsHi3::AtFtsHi3::3XHA* and *35S::AtFtsHi3::GFP*) were transformed into electro-

competent *Agrobacterium tumefaciens*(GV3101::pMP90 (pTiC58DT-DNA); (Hellens et al., 2000). WT (Col-0) plants were transformed with these constructs by the floral dip method described by Clough and Bent (1998). The presence of the construct in the T1 and T2 generation was confirmed by germinating transgenic seeds on 35 mg ml^{-1} hygromycin-B selecting MS agar plates. The experiments were performed on T2 generation seeds.

2.3 | Water stress analysis

Wild-type and transgenic plants were grown on soil in the growth chamber under short-day conditions (8 /16 h photoperiod, 22/18°C, relative humidity 50% and 120 μmol photons m^{-2} s^{-1}) with regular watering for 3–4 weeks before treatment. Long-term water stress analyses were performed by withdrawing watering for 15 days until the drought effects were observed in the Wt or the overexpressor lines. The experiments were performed three times.

2.4 | Drought tolerance assay

To assay drought tolerance, the 'one rosette per-pot' and 'weighing' methods were used as described by (Harb and Pereira, 2011; De Ollas et al., 2019, Mishra et al., 2021). Two-week-old, plate-grown, WT and overexpression seedlings (15 replicates) were transplanted to 5 cm pots containing a 3:1 mixture of commercial soil (Hasselfors garden special, Sweden) and Vermiculite (Sibelco, Europe), and plants were grown in a growth chamber under short-day conditions (8 /16 h photoperiod, 22/18°C). Initial daily transpiration was calculated on pots saturated with 500 mL water (15 pots per tray) and weighed for 5 to 6 days to determine the soil water volumetric content. Rosette diameters were measured at 3–4 day intervals throughout the experiment. Drought was induced at 37 days (23 days following transplantation), and pots were weighed daily between 9 and 11 am to calculate the water deficit. After 15 days of drought stress, plants were rewatered for three days, and rosette fresh weight (FW) was recorded. Rosettes were subsequently placed in glassine bags and oven-dried at 65°C for 72 h to obtain dry weight (DW). Leaf water content (%) was calculated as: (FW-DW/FW). Statistical analysis was conducted using Student's t-test.

2.5 | Abscisic Acid Extraction and Quantification

Sample preparation and extraction for Solid Phase Extraction (SPE) and ultra-high performance liquid chromatography-mass spectrometry (UHPLC–MS/MS) were performed as described by Haas et al. (2021). Statistical analysis was conducted using Student's t-test.

2.6 | Phenotypic characterization

Wild type and *pFtsHi3-OE1 and pFtsHi3-OE2* seedlings were investigated at the age of ten days using a Leica MZ9.5 stereomicroscope or scanned by Epson Perfection 3200 PHOTOscanner. Plants grown on soil or exposed to stress conditions were photographed at the age of six weeks using a Canon 650D camera. Statistical analysis was conducted using Student's *t*-test.

2.7 | RNA extraction, cDNA synthesis, and quantitative PCR (qPCR)

Total RNA was extracted from leaves of three biological replicates of 10-day and 6-week-old wild-types and overexpressors, using an RNA-queous Total RNA Isolation Kit (Invitrogen). Isolated RNA was reverse transcribed into cDNA using a RevertAid First Strand cDNA Synthesis Kit (Thermo Scientific). Quantitative RT-PCR was performed using a BioRad CFX96 thermocycler. Cq-values were obtained using the CFX Maestro software (BioRad) and the data were analysed using the BioRad CFX Manager 3.1 software (Mishra et al., 2019). The 2-CT method was employed to calculate relative quantification values for each target gene. Data were normalized to the expression of the housekeeping genes. Statistical analysis was conducted using Student's t-test. The housekeeping genes (ubiquitin, tubulin, and actin, Czechowski et al., 2005) and gene-specific qPCR primers are listed in Table S7.

2.8 | Leaf-level gas exchange

A portable photosynthesis system (Li-6400xt, Li-Cor) was used to determine the photosynthesis rate (assimilation *AN*) and stomatal conductance (*gs*) as described by (Tomeo and Rosenthal, 2018). Detailed steps are mentioned in (Mishra et al., 2021). Statistical analysis was conducted using Student's t-test.

2.9 | Chloroplast size and ultrastructure

TEM was used to study the chloroplast morphology of the first true leaf of 12-day-old seedlings of WT and *pFtsHi3-OE1 and pFtsHi3-OE2 lines*. Sample preparation and microscopy were performed at the Umeå Centre of Electron Microscopy (UCEM). The open-source image-processing program ImageJ (Java-based image-processing program developed at the NIH) measured chloroplast length and width. Statistical analysis was conducted using Student's t-test.

2.10 | Mass spectrometry-based proteomics (shotgun)

2.10.1 | Sample preparation

Arabidopsis proteome samples were prepared from leaf tissue harvested from watered and drought-treated WT, *ftshi3-1* and *pFtsHi3-OE* plants grown as mentioned in the drought tolerance section. Five replicates per genotype per treatment were pooled and five technical replicates were used. The harvested plant material (500 mg) was inserted in 2 mL

Eppendorf tubes with glass beads and frozen in liquid N$_2$. The tissue was homogenized using a TissueLyser at 30 Hz for 1 min and refrozen in N$_2$. Proteins were extracted in 3 volumes of prechilled ($-20°$C) precipitation solution (TCA 10% and Acetone 90%) and precipitated at $-20°$C overnight. The proteins were pelleted by centrifugation at 14,800 g for 15 min at 4°C and the supernatant was discarded. The pellet was then washed with 500 μL ice-cold acetone and centrifuged again as above. The washing step was repeated 3 times to remove residual TCA and acetone, and the pellet was dried at room temperature and stored at $-80°$C.

TCA-precipitated proteins were resuspended in 45 μL 8 M urea buffer (5 mM EDTA, 100 mM NH4HCO3, 1 mM DTT, pH 8.0). The total protein concentration was determined using the BCA protein assay kit (ThermoFisher Scientific). Subsequently, 15 μg total protein per sample was reduced (10 mM DTT, 30 min, 30°C), carbamidomethylated (55 mM CAA, 30 min, room temperature) and digestion with trypsin (proteomics grade, Roche) overnight at 37°C at a 1:50 enzyme: protein ratio (w/w). Digests were acidified by the addition of 0.5% (v/v) formic acid (FA) and desalted using self-packed StageTips (three disks per microcolumn, ø 1.5 mm, C18 material, 3 M Empore). The peptide eluates were dried to completeness and stored at $-80°$C. For LC–MS/MS analysis all samples were re-suspended in 75 μL 2% acetonitrile (ACN) and 0.1% FA in HPLC grade water and 2 μL sample volume were injected into the mass spectrometer per mass spectrometric (MS) measurement.

2.10.2 | LC–MS/MS data acquisition

LC–MS/MS measurements were performed on a nanoLC Ultra1D+ (Eksigent) coupled online to a Q-Exactive HF-X mass spectrometer (ThermoFisher Scientific). Peptides were loaded onto a trap column (ReproSil-pur C18-AQ, 5 μm, Dr. Maisch, 20 mm $\times$ 75 μm, self-packed) at a flow rate of 5 μL min^{-1} in 100% solvent A (0.1% FA in HPLC grade water). Subsequently, peptides were transferred to an analytical column (ReproSil Gold C18-AQ, 3 μm, Dr. Maisch, 400 mm $\times$ 75 μm, self-packed) and separated using a 50 min linear gradient from 4 to 32% of solvent B (0.1% FA in ACN and 5% (v/v) DMSO) at 300 nL min^{-1} flow rate. Both nanoLC solvents contained 5% (v/v) DMSO. The Q-Exactive HF-X was operated in data-dependent acquisition (DDA) mode, automatically switching between MS1 and MS2 spectrum acquisition. MS1 spectra were acquired over a mass-to-charge (m/z) range of 360–1300 m/z at a resolution of 60,000 using a maximum injection time of 45 ms and an AGC target value of 3e6. Up to 18 peptide precursors were isolated (isolation window 1.3 m/z, maximum injection time 25 ms, AGC value 1e5), fragmented by high-energy collision-induced dissociation (HCD) using 26% normalized collision energy and analyzed at a resolution of 15,000 with a scan range from 200 to 2000 m/z. Precursor ions singly charged, unassigned, or with charge states >6+ were excluded. The dynamic exclusion duration of precursor ions was 25 s.

2.10.3 | LC–MS/MS data analysis

Peptide and protein identification and quantification were performed using MaxQuant (version 1.6.17. 0) with its built-in search engine Andromeda (Cox et al., 2011; Tyanova et al., 2016). MS2 spectra were searched against an Arabidopsis proteome fasta file downloaded from TAIR (48359 protein entries, downloaded April 2017) supplemented with common contaminants (built-in option in MaxQuant). Carbamidomethylated cysteine was set as a fixed modification and oxidation of methionine and N-terminal protein acetylation as variable modifications. Trypsin/P was specified as the proteolytic enzyme. The precursor tolerance was set to 4.5 ppm, and fragment ion tolerance to 20 ppm. Results were adjusted to 1% false discovery rate (FDR) on peptide spectrum match (PSM) and protein level, employing a target-decoy approach using reversed protein sequences. The minimal peptide length was defined as 7 amino acids. The "match-between-run" function was disabled. Label-free protein quantification (LFQ values) was used in downstream data analysis with the software Perseus (Tyanova et al., 2016). LFQ values were log-transformed (base 2) and median-centred, followed by filtering proteins based on minimally one detected LFQ value throughout five biological replicates within at least one condition. Subsequently, the imputation of missing values was performed with Perseus using the function "replace missing values from normal distribution" (width = 0.3, downshift = 1.8, default settings). The functional annotation of proteins was downloaded from TAIR. The protein differential expression analyses were performed using the student's t-test. The resulting p-values were corrected using the Benjamini and Hochberg method to control FDR (0.01) for differential expression. Gene ontological analysis was conducted using PANTHER (pantherdb.org), and string plots were generated using STRING (string-db.org). A list of significant AGIs from our comparisons can be found in the supplement (Table S8-10).

2.11 | Modelling methods

To receive clues in the absence of mechanistic information about the different phenotypes arising with different amounts of FtsHi3 in the plant cell, we developed a mathematical approach that captured the essential features of protease heteromer-formation with a sampling-based exploration of the model space. We made assumptions based on observations of FtsH proteases in other membranes, in particular, we assumed that AtFtsHi3 binds specific partners to form hetero-hexameric complexes (Moldavski et al., 2012). For simplicity, we assumed that each such heteromeric structure is formed by only two types of compounds in specific stoichiometric ratios of 1:1. In principle, hexamers could be formed in many possible ways, such as through sequential binding of proteases one at a time (Nauta and Miller, 2000) or through combinations of larger structures such as dimers or trimers (Prokhorova and Blow, 2000). If we considered all such modes of forming hexamers, then the parameter space would increase significantly, and our results would conflate the effects of binding interactions with the mechanism of hexamer formation. Thus, we made the simplifying assumption that hetero-hexamers are composed of two different subunits, which means that our model applies to any system in which basic components are combined in pairs, e.g. monomers forming dimers or trimers forming hexamers. Without knowledge of which FtsH subunits bind to each
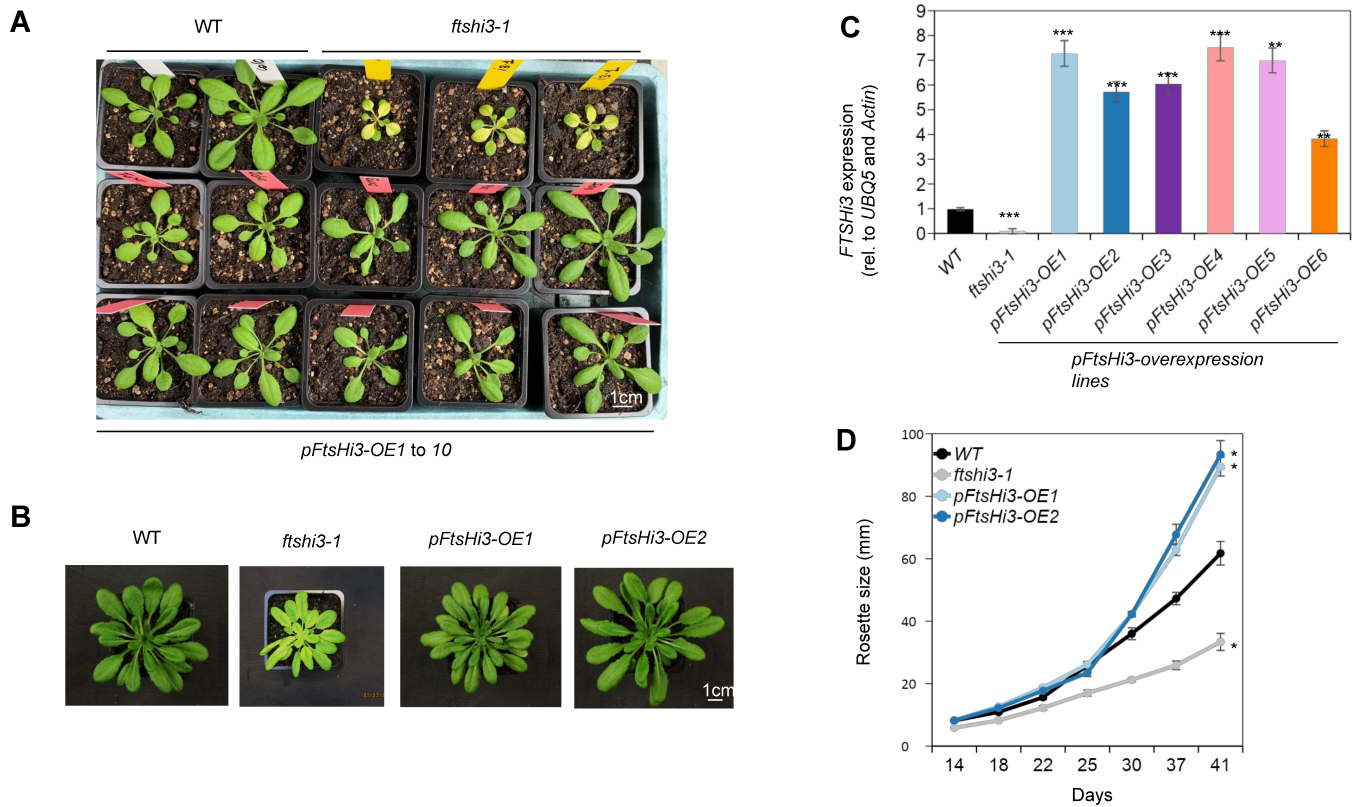
FIGURE 1 **A**, Phenotypes of WT (top left, white labels), *ftshi3-1* (top right, yellow labels) and *pFtsHi3-OE1 to -OE10* (middle and lower rows, red labels) at 3 weeks of age under long day (LD) conditions (16/8 hr D/N cycle, 22°C). **B**, Phenotypes of WT, *ftshi3-1* and two representative overexpressor lines (*pFtsHi3-OE1* and *-OE2*) at 6 weeks of age under SD conditions (8/16 hr D/N cycle, 22°C). **C**, Expression of *FtsHi3* relative to *UBQ5* and *actin* in *pFtsHi3-OE* lines at 3 weeks of growth under short day (SD), soil grown conditions (n = 3). **D**, Rosette diameter of WT, *ftshi3-1*, *pFtsHi3-OE1* and *-OE2* under the same conditions as B (n = 8). Data are means # standard error, asterisks indicate significance; $p < 0.05$ (*), $p = 0.01$ (**), $p < 0.001$ (***) and scale bars are as indicated.

other, we constructed a set of all possible interaction diagrams (17 different diagrams) for systems with 3 or 4 proteases that could result in heteromeric complexes. Determining the typical qualitative dynamics of each interaction diagram would identify protease-binding interactions that could produce the experimental observations. We determined the typical qualitative dynamics of an interaction diagram by studying its corresponding system of differential equations. Each interaction diagram of 3 or 4 proteases can be translated into a system of 3 or 6 differential equations. In the absence of information concerning the reaction kinetics of binding, we determined the typical behaviour through a sampling procedure. We randomly sampled reaction rates using a uniform distribution between (0,1) and initial protease concentrations using a uniform distribution between (0,10). For each random set of parameters, we solved the differential equation system to find the steady-state concentrations of hexameric complexes. We then used subunit A as a proxy for AtFtsHi3 and repeated the steady state calculation after increasing/decreasing its initial concentration by a factor of 100, representing the effects of overexpression/knockdowns. We assessed whether increasing the concentration of FtsHi3 (or A) resulted in: 1. an increased proportion of steady-state concentration of A complexes and 2. non-monotonic behaviour in the proportion

of complexes containing any other protease. The requirement for non-monotonic behaviour was that the proportion of complexes formed by a protease should be high-low-high or low-high-low with increasing concentration of subunit A. We calculated the average occurrence of each qualitative behaviour for an interaction diagram using 10 samples of 100 sets of random parameters.

3 | RESULTS

3.1 | Characterization of *Arabidopsis* plants with elevated expression of *AtFtsHi3*

To understand the role of the chloroplast-envelope located pseudo-protease AtFtsHi3 in overall plant development, we generated two sets of *AtFtsHi3* overexpression lines: one set expressing an additional *FtsHi3* gene under the control of its native, endogenous promoter (*pFtsHi3-FtsHi3OE*, termed **p***FtsHi3-OE*) (Figure 1) and one set overexpressing *FtsHi3* under the constitutive *35S* promotor (*35SFtsHi3-FtsHi3OE*, termed **35S***FtsHi3-OE*) (Figure S1). *AtFtsHi3* transcript levels were determined in these lines; the *pFtsHi3-OE* lines showed approximately 4- to 8-fold expression of *AtFtsHi* relative to the WT
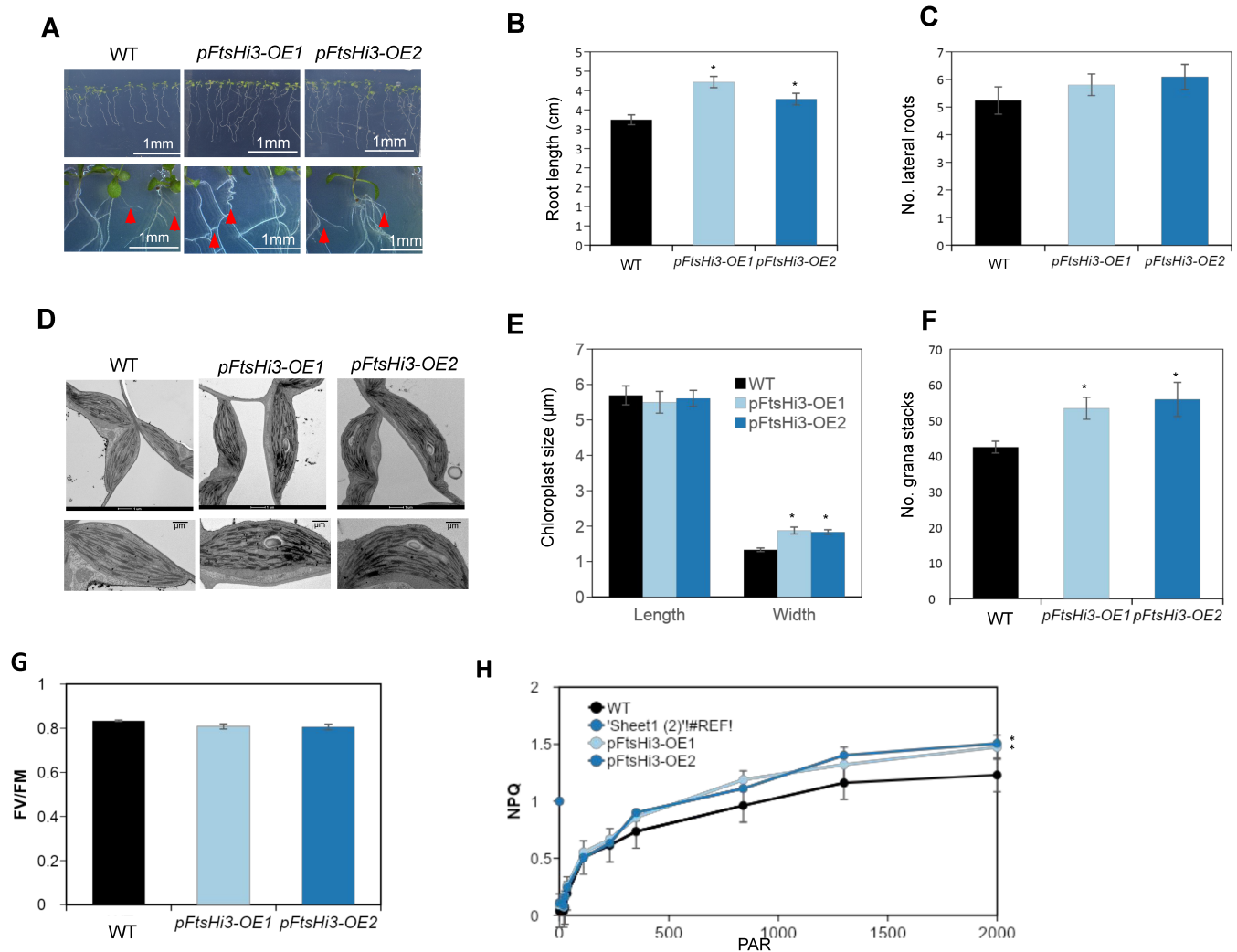
FIGURE 2 **A**, Root phenotype of 8-day-old seedlings from WT, *pFtsHi3-OE1* and *pFtsHi3-OE2*. Arrows indicate the lateral roots. **B**, Root length of 8-day-old seedlings (n = 25). **C**, Number of lateral roots of 8-day-old seedlings (n = 21). **D**, Transmission electron micrographs showing chloroplasts (upper panel) and zoomed-in ultrastructures (lower panel) of the first true leaves in seedlings of WT, *pFtsHi3-OE1* and *pFtsHi3-OE2*. **E**, Size of chloroplasts from first true leaves in WT, pFtsHi3-OE1 and pFtsHi3-OE2 lines (n = 40). **F**, Number of grana stacks per chloroplast (n = 40); **G**, Chlorophyll fluorescence (FV/FM); **H**, non-photochemical quenching (NPQ) of WT, *pFtsHi3-OE1* and *pFtsHi3-OE2*. Plants were grown at SD conditions (8/16 hr D/N cycle, 22°C). Data are means # standard error, significances; p < 0.05 (*) and scale bars are as indicated.
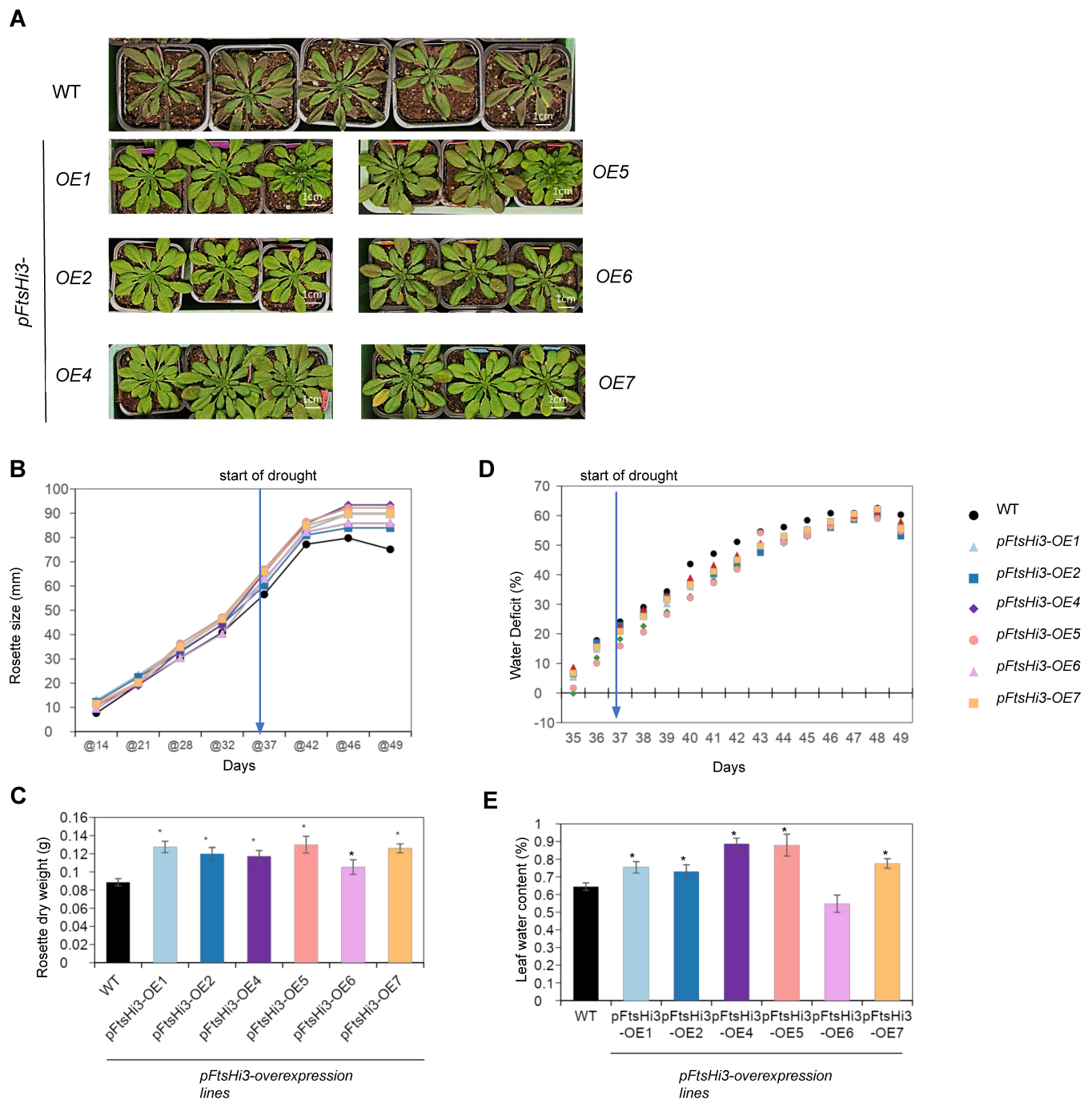
(Figure 1C). Transcription of *FtsHi3* in the *35SFtsHi-OE* lines was typically doubled compared to WT (Figure S1C).

Under short-day growth conditions, which inhibit bolting, overexpression lines appeared similar to the WT as seedlings, but their rosettes grew significantly larger at later growth stages (Figure 1D, *p* < 0.05; Figure S1B). A similar growth pattern was observed under long-day conditions (data not shown). We further observed significantly larger root growth (around 20%) (Figure 2A-B) and a slightly increased number of lateral roots in *pFtsHi3-OE1* and *pFtsHi3-OE2* (Figure 2C) compared to WT. Contrary to *ftshi3-1* (Mishra et al., 2021), chloroplasts in the first true leaves of *pFtsHi3-OE1* and *pFtsHi3-OE2* lines displayed fully developed ultrastructures (Figure 2D) with increased width (Figure 2E) and an elevated number of thylakoid membranes and significantly higher degree of grana

stacking (Figure 2F). While the photosynthetic performance showed no remarkable disparity (FV/FM values, Figure 2G), non-photochemical quenching was higher in *pFtsHi3-OE* lines (Figure 2H). This implies that NPQ may enhance photosynthesis and bolster the ability to eliminate ROS in the overexpressor lines.

3.2 | Overexpression of *AtFtsHi3* confers drought tolerance without penalizing plant growth

We investigated the response to drought stress in six overexpressor lines under the endogenous promotor (*pFtsHi3-OE*, Figure 3) and in three overexpressor lines under the constitutive *35S* promotor (*35SFtsHi-OE* lines, Figure S2A) and compared to WT. Plants were

FIGURE 3 Effect of drought on WT and *pFtsHi3-OE* lines grown on soil. **A**, Representative post-drought phenotypes of WT, *pFtsHi3-OE1, 2, 4, 5, 6, 7* plants exposed to drought stress for 15 days under SD conditions (8/16 hr D/N cycle, 22°C). **B**, Expression of *FtsHi3* relative to *UBQ5* and *actin* in WT, the knock-down mutants *ftshi3-1* and the overexpressor line *pFtsHi3-OE1* line in watered conditions and after 15 days of drought stress (n = 3). **C**, Rosette diameter prior to, and following drought induction at day 37. **D**, Dry weight of harvested rosettes following drought. **E**, Progressive % water deficit during drought. **F**, Calculated leaf water content %: (Biomass of watered control) - (Biomass of droughted) / (Biomass of watered control). Data are means # standard error (n = 15), significances; p < 0.05 (*).

germinated on plates containing MS + 1% sucrose and, after 7 days, transferred to pots. After 30 days of growth, the plants were exposed to drought for 15 days. Transcription of *AtFtsHi3* was observed to be stronger during drought stress in WT and significantly stronger in the overexpression lines (Figure 3B). While WT displayed severe symptoms of drought, the overexpressor lines retained healthy phenotypes

(Figure 3A) throughout the 15-day drought period. We observed a significant reduction in wilting across all OE lines (Table S1). Similar results were achieved when the pots were randomized within the same tray ("one-pot" experiment) to give them all access to the same amount of water (Figure S2B, C). The *pFtsHi3-OE* lines had larger rosettes and higher final biomass (Figure 3C, D) than WT. The level of water deficit

during progressive drought was similar between the WT and *pFtsHi3-OE* lines (Figure 3E), although WT exhibited a slightly higher deficit. Most of the overexpression lines had higher leaf water content than WT plants (Figure 3F, Figure S2G). The *35SFtsHi3-OE* lines displayed similar drought-tolerance to the pFtsHi3-OE lines, however, they continued to grow during the entire drought period (Figure S2D), leading to further increases in their final dry weights (Figure S2E). They displayed greater variability and showed higher water deficits towards the end of the experiment (Figure S2F).

3.3 | Gas exchange qualities, stomatal physiology and ABA response are altered in *pFtsHi3-OE* lines

Gas exchange parameters are expected to decline in plants during drought. Gas exchange parameters were assessed on WT, *pFtsHi3-OE1* and *-OE2* as well as *35SFtsHi3-OE5, -OE7* and *-OE8* before (37-day-old) and after the 15-day drought period (Table S2). Prior to the drought, net photosynthesis (AN) and stomatal conductance (gs) showed variability among all genotypes, while the CO_2 concentration inside the leaf (Ci) remained consistent. After 15 days of drought, WT exhibited significantly lower AN and gs than the OE lines (Table S2). Notably, Ci values were elevated in WT, but decreased in the OE lines during drought. Water use efficiency (WUE intrinsic), indicated by the ratio AN/gs, significantly increased in all overexpression lines during drought treatment (Table S2).

Drought stress activates ABA-biosynthesis, leading to the expression of ABA-responsive genes, which can be signalled either via an ABA-dependent or an ABA-independent pathway or by cross-talk between both pathways (Yoshida et al., 2014). We examined abscisic acid (ABA) levels before and after drought in WT and *pFtsHi3-OE* representative lines. While ABA levels were similar across all genotypes before drought (Figure S3A), *pFtsHi3-OE* lines responded to drought with a less pronounced increase (~2-fold) compared to the WT (~6-fold increase, Figure S3A). The average density of stomata per mm² was 252 in WT, 200 in *pFtsHi3-OE1*, and 204 in *pFtsHi3-OE2* (Figure S3B,C). Additionally, the OE lines had reduced stomatal size (width to length ratio) compared to WT (18.9 by 14.9 μm for WT, 17.5 by 13.9 μm for *pFtsHi3-OE1*, and 16.7 by 12.1 μm for *pFtsHi3-OE2*). Stomatal closure in response to 10 μM exogenous ABA treatment showed similar responses in all lines (Figure S3D, E).

We hypothesized that the altered levels of ABA in *pFtsHi3-OE1* and *pFtsHi3-OE2* under drought conditions might affect the expression of ABA-responsive genes. The expression patterns of nine ABA-responsive genes were therefore investigated in both drought and watered conditions (Table S3). The marker genes *Responsive-to-desiccation 29A*, and *22 (RD29A, RD22), Dehydration-responsive-element-binding-protein and 2A (DREB2A), Cold-regulated 47 (COR47)* and *Drought-induced 21 (DI21)* all displayed consistently higher expression in the *pFtsHi3-OE* lines under watered conditions. However, during drought, RD29B, DREB2A, and COR47 showed significantly elevated expression in WT, but the expression did not change in the *pFtsHi3-OE* lines. This aligns with the reduced accumulation of

endogenous ABA observed under drought and suggests that the *pFtsHi3-OE* plants perceive a state of drought even under watered conditions despite having normal ABA levels. Interestingly, RD22 displayed reduced expression in WT upon drought onset, while its expression was significantly increased in the *pFtsHi3-OE* lines.

3.4 | Plants with modulated AtFtsHi3 content show changes in proteome composition during water deficit

Changes in the abundance of AtFtsHi3 seem to induce drought tolerance in *Arabidopsis thaliana*. While the lack of AtFtsHi3 (*ftshi3-1*) results in a chlorotic, dwarf phenotype (Mishra et al., 2021), it is noteworthy that the heightened expression of this pseudo-protease leads to plants exhibiting phenotypes comparable to or even surpassing those of the wild type, emphasizing the impact of *AtFtsHi3* expression. To explore the effect of AtFtsHi3 on drought tolerance, we compared the proteomes of *ftshi3-1*, *pFtsHi3-OE1* and WT leaves under both watered and drought conditions. Using an S0 threshold of 2 (Effectively minimum fold change) and a false discovery rate (FDR) adjusted t-test *p*-value cutoff of 0.01, we observed a number of proteins with altered abundance in selected comparisons; *ftshi3-1* vs WT under drought conditions: 762, *ftshi3-1* vs WT under watered conditions: 140, and *pFtsHi3-OE1* vs WT under drought conditions: 75 (Figure 4A-C). Interestingly, we did not observe any peptides that showed differential abundance in the comparison between watered *pFtsHi3-OE1* and WT plants (Figure 4D). This suggests that there is no apparent functional difference in the protein composition between the WT and *pFtsHi3-OE1* lines under watered conditions. Despite the overexpression of FtsHi3 in *pFtsHi3-OE1* under control and drought conditions (Figure 3B), we could not detect any peptides corresponding to AtFtsHi3.

While the *AtFtsHi3* overexpression lines, as well as the *AtFtsHi3* knock-down line *ftshi3-1* (Mishra et al., 2021) are drought-tolerant, the growth phenotype of both mutations differs significantly (Figure 1B). AGIs (Arabidopsis Genome Initiative) altered explicitly in the *ftshi3-1* mutant compared to *pFtsHi3-OE1* and WT, therefore, should possibly identify growth-related processes. At the same time, AGIs are common to both *ftshi3-1* and *pFtsHi3-OE1* but different from WT and should be associated with drought resistance. The differentially abundant protein lists were therefore further compared to segregate AGIs and identify elements common to major contrasts (Figure 4E). Most (61 of 75) differentially abundant proteins from the *pFtsHi3-OE1* vs WT comparison in drought conditions (Figure 4C) were also detected in the *ftshi3-1* vs WT comparison (Figure 4A). 97 AGIs were shared by the *ftshi3-1*: WT comparisons in watered and drought conditions. However, only seven AGIs were shared between the droughted *pFtsHi3-OE1*: WT and the watered *ftshi3-1*: WT contrasts. These seven AGIs include ribosomal proteins (ATCG01120, AT3G53740, AT2G37600, AT4G15000), a protein responsible for cell wall integrity (AT5G66090), a mitochondrial protein of the adenylate kinase family (AT5G50370) and an NADH dehydrogenase family protein (ATCG01100).
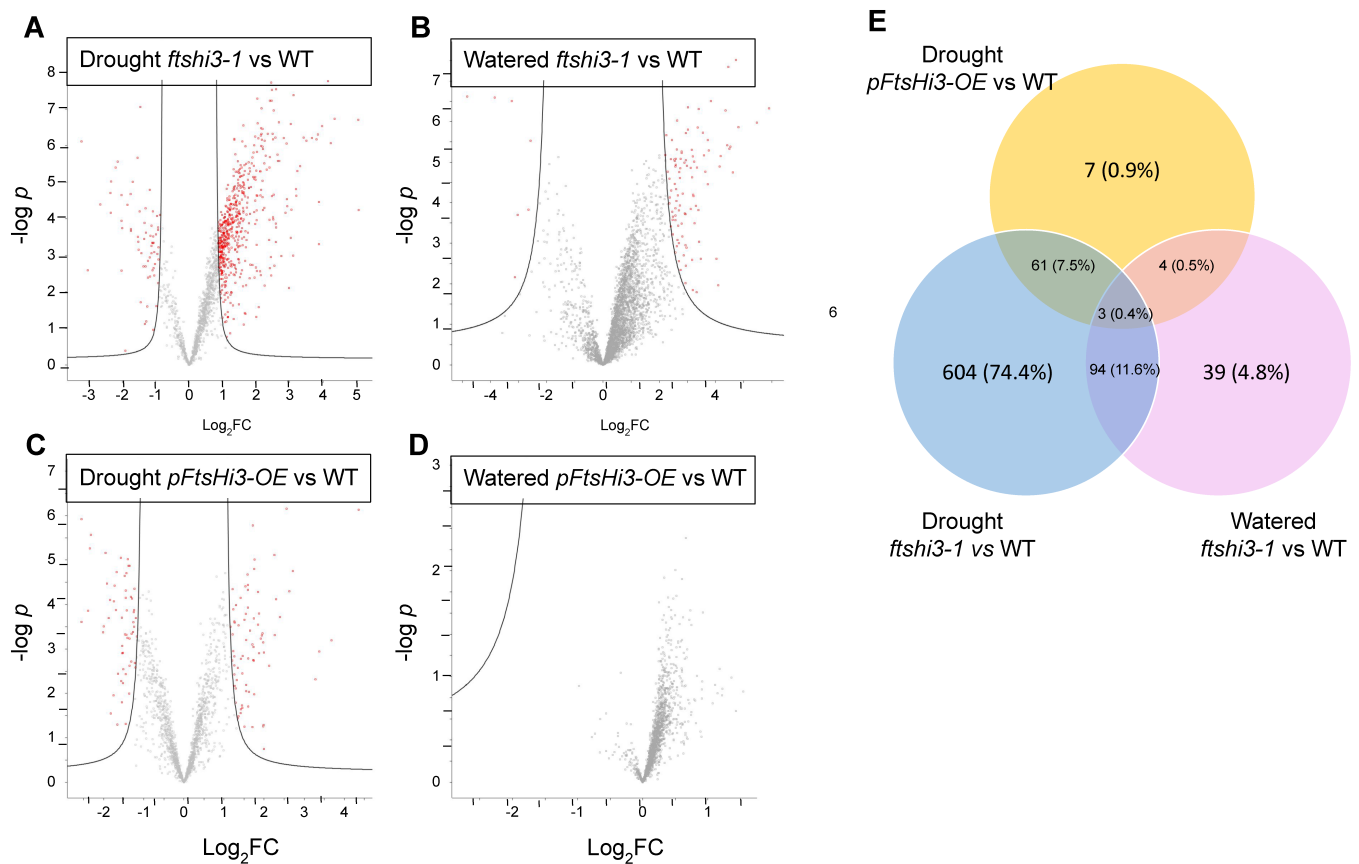
FIGURE 4 Volcano plots showing the number of proteins with statistically altered abundance in **A**, *ftshi3-1* vs WT under drought conditions; **B**, *ftshi3-1* vs WT under watered conditions; **C**, *pFtsHi3-OE1* vs WT under drought conditions; **D**, *pFtsHi3-OE1* vs WT under watered conditions. Data are log fold change (X-axis) vs -logo of the corresponding p-value, with an SO cutoff of 2 and an FDR cutoff of 0.01 (regression lines). **E**, Venn Diagram showing the number of overlapping differentially abundant proteins in *ftshi3-1* vs WT under drought and watered conditions and their relationship to *pFtsHi3-OE1* vs WT.

Ontological analyses were performed on these AGI lists to highlight enriched biological processes (Tables S4-6). In the AGI list of peptides elevated only in the *ftshi3-1* mutant under drought conditions, various processes related to photosynthesis were found to be overrepresented, such as protoporphyrinogen IX biosynthesis, chlorophyll biosynthesis, chloroplast rRNA processing, chloroplast protein import, thylakoid membrane organization, and chloroplast organization (Table S4). Isoprenoid metabolic processes (geranylgeranyl diphosphate biosynthesis, geranyl diphosphate metabolism, and farnesyl diphosphate biosynthesis) and amino acid biosynthetic processes (Valine, Isoleucine, Leucine, Lysine biosynthesis) were also enriched in *ftshi3-1*. On the other hand, the repressed AGI list specific to *ftshi3-1* showed significant enrichment in inositol biosynthesis, anthocyanin-containing compound biosynthesis, and phenylalanine catabolism (>100-, 96.56-, and 86.91-fold, respectively) (Table S5). Interestingly, we also observed the repression of several drought-associated processes, such as response to desiccation and response to abscisic acid (ABA), suggesting that *ftshi3* mutant plants may be partially repressing drought responses compared to the WT.

To visualise the ontological processes identified above, we constructed STRING plots (string-db.org) to explore known protein–protein interactions within the AGI lists specific to the *ftshi3-1* line. We observed three large clusters in the elevated protein list (Figure S4, High confidence interactions, MCL, Inf = 2) corresponding to tetrapyrrole (chlorophyll and heme) biosynthesis, chloroplast organization and RNA processing. We also saw several smaller clusters that included protein trafficking enzymes (TICs and TOCs) as well as affiliated chaperone elements (CR88 and HSP70). In the AGI STRING plot showing protein–protein interactions between proteins repressed in *ftshi3-1* relative to WT under drought conditions (Figure 5) we observed clusters of known drought/cold-responsive proteins (such as LEA14 and COR47), flavonoid biosynthesis proteins (e.g. TT4/TT5) and photosynthetic proteins (e.g. the PsbQ-like proteins PnsL2/3) as well as a distinct cluster containing all three inositol 3-phosphate synthase proteins, which catalyze the rate-limiting step of myo-inositol biosynthesis (Donahue et al. 2010).

In the ontological analysis of AGIs common to *ftshi3-1* and *pFtsHi3-OE1* (Table S6), enzymes involved in proton transmembrane transport and response to water deprivation were highly enriched (43- and 21-fold, respectively). Additionally, the processes; response to cold, response to abscisic acid and response to osmotic stress,
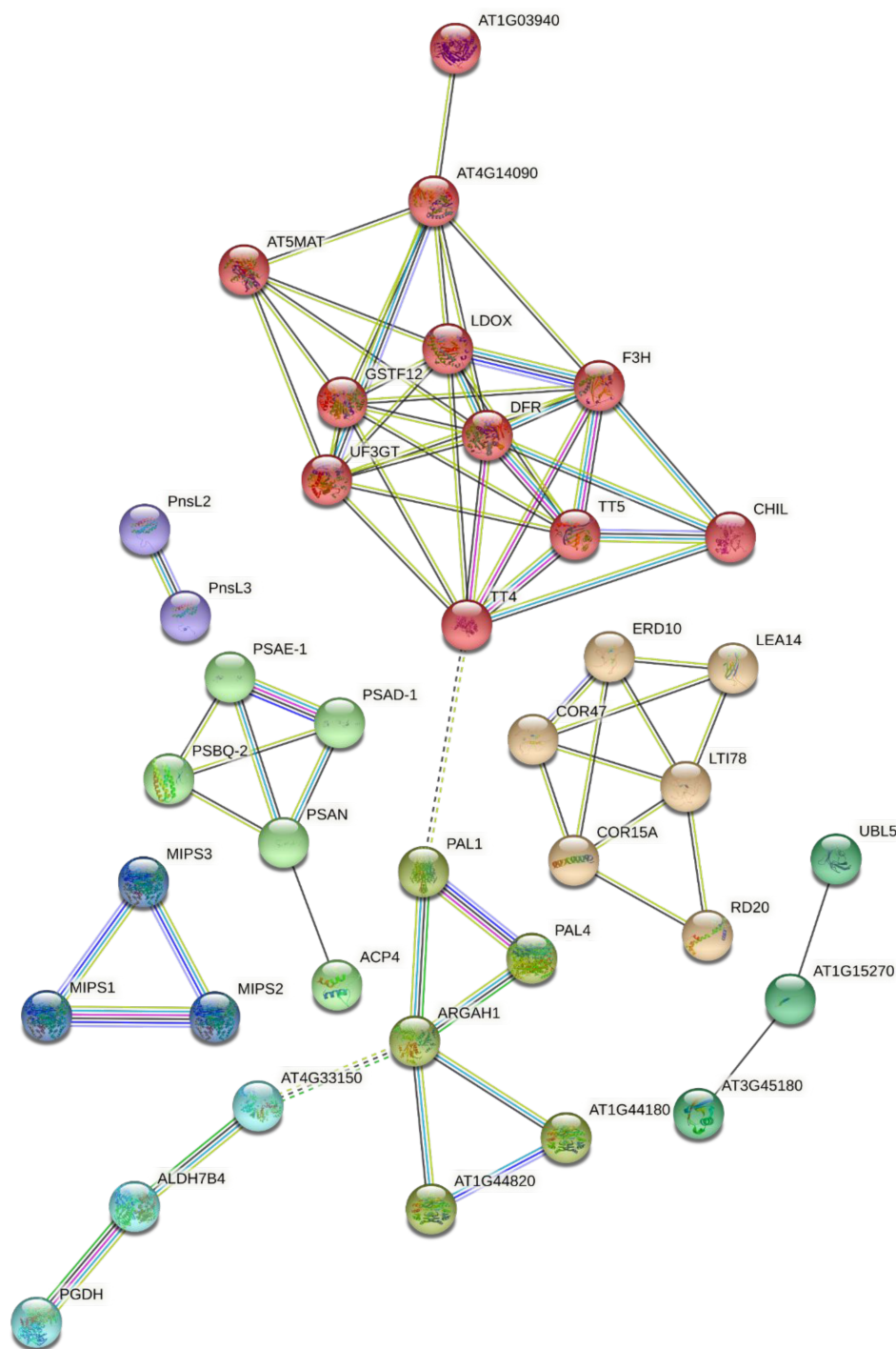
FIGURE 5 STRING plot showing protein:protein interactions between proteins repressed in *ftshi3-1* relative to WT under drought conditions. Data were filtered to retain only high confidence interactions (0.700) and disconnected nodes were removed. The resulting elements were clustered using an MCL inflation parameter of 2. Clusters are distinguished by node color and line color indicates number and type of evidence for interactions (see string-db.org/), dashed lines indicate borders of clusters. Protein names or AGIs are provided adjacent to nodes.

were also strongly enriched. Given that the osmotic stress-related processes are composed of AGIs that are repressed in both the *pFtsHi3-OE1* and *ftshi3-1* contrasts, this suggests that these processes may be responsible for conferring drought resistance to the *pFtsHi3-OE1* and *ftshi3-1* lines. Further exploration of these groups reveals quite a small number of AGIs present in several of these categories. To visualize their relative abundances (based on log LFQ values), we constructed a heatmap to compare the droughted WT, *pFtsHi3-OE1* and *ftshi3-1* lines as well as the watered WT (Figure 6). The abundances of the ABA inducible KIN1, the AKR4C9 aldo-keto

reductase, the ABCG30/36/37 transporters and the Late Embryogenesis Abundant protein LEA4-5 appeared juxtaposed between the WT and the *pFtsHi3-OE1/ ftshi3-1* lines, while the abundance of the thiamine biosynthesis protein THI1 was increased more so in *ftshi3-1* than *pFtsHi3-OE1*. Relative to the drought-stressed WT, we also found protein abundance of the putative chitinase CHI, LEA7, a lipid transfer protein: LTP4, AKR4C8, a drought-responsive protein LTI65 (RD29B), a GTPase RAB18, and alcohol dehydrogenase ADH1 to be repressed in both *ftshi3-1* and *pFtsHi3-OE1*, but this was more severe in the OE line.

FIGURE 6 Heatmap showing mass spectrometric intensities ($\log_{10}$ LFQ) of AGIs that were differentially abundant in both *pFtsHi3-OE1* and *ftshi3-1* lines relative to the WT under drought conditions (S0 > 2, p-value <0.01). Dendrograms represent dissimilarities between contrasts (above) and proteins (left).
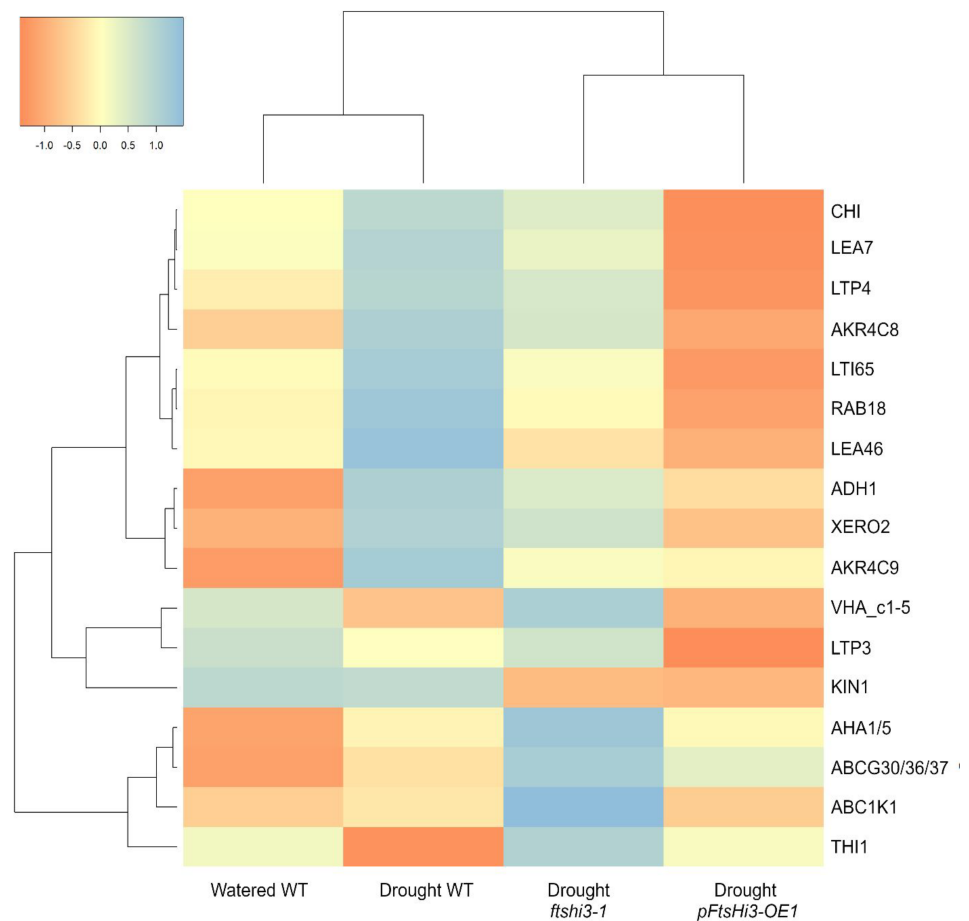
3.5 | Changes in transcript abundance of *AtFtsHi3* lead to drought tolerance but affect plant growth differently in overexpressor and knock-down mutant lines: A model

FtsH proteases are known to form hexamers. A variety of homo- or heteromeric complexes would provide a possible mechanism that could explain how differential expression of the AtFtsHi3 pseudo-protease induces characteristically different phenotypes: decreasing growth rate with lower expression (monotonic behaviour) and increasing drought resistance with lower as well as higher expression (non-monotonic behaviour). We, therefore, created a mathematical model to identify the minimal number and types of interactions between AtFtsHi3 and possible complex partners and/or substitutes that would recapitulate our experimental observations. The model was based on the following simplifying assumptions to produce a more general model: Each heteromeric structure is formed by only two types of homo-trimers in specific stoichiometric ratios of 1:1. We also assumed that both growth rate and drought resistance are determined by the relative abundance of different heteromeric complexes - thus it is not just the absolute amount of a specific protease, but its proportion in the membrane. We then considered a range of different biochemical models with varying numbers of FtsHi/FtsH subunits forming hexamers (3 or 4, less than 3 could not generate the behaviour) and types of

interactions (see Method section). Using a random sampling method based on (Libby & Lind, 2019) , we identified which models (number of protease subunits and types of interactions) are most likely to reproduce our experimental findings (Figure 7).

All models could recapitulate the monotonic behaviour of growth because complexes that involved the AtFtsHi3 pseudo-protease naturally increased with increasing expression of AtFtsHi3. In contrast, the non-monotonic behaviour of drought tolerance was less often observed in our models (Figure 7B). A common feature of those models with non-monotonic behaviour was that FtsH proteases, especially AtFtsHi3, interact with multiple partners. Allowing different proteases to belong to several different heteromeric complexes creates opportunities for competitive binding that could shift the proportions of complexes (see Figure 7C, D). In models where AtFtsHi3 had a single specific partner, we did not observe non-monotonic behaviour. We explored the robustness of the findings of our mathematical model for different parameter regimes by studying the dynamics for all 17 possible complex interactions, including 3 or 4 subunits (Figure S5). The reader should note that the interactions in panels B) and L) stand out with having zero detected monotonic behaviour. In these interactions, all complexes contain the 'A' homo-trimer; therefore the proportion of the 'A' subunit equals 1 for each line (WT, *ftshi3-1* or *pFtsHi3-OE1*). Besides these two special cases, monotonic behaviour is detected
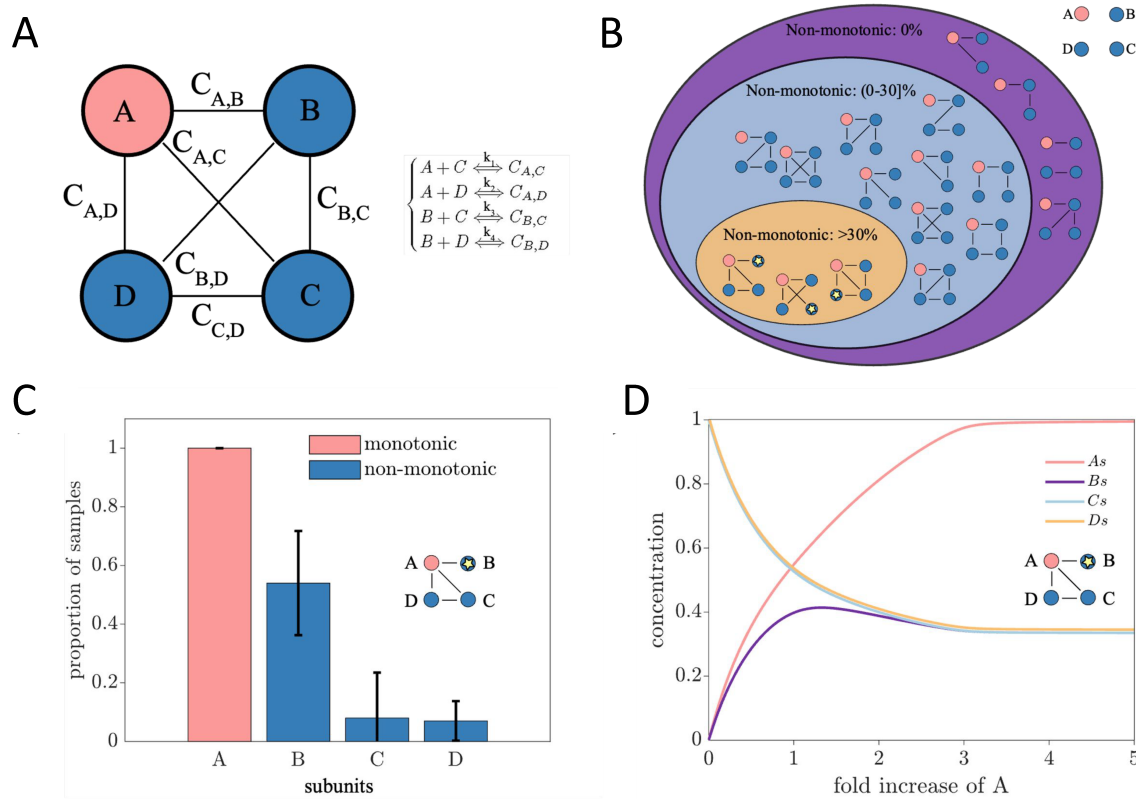
FIGURE 7 Mathematical modelling to explain the phenotypic variation concerning growth and drought tolerance of *FtsHi3* mutant lines. **A,** Scheme showing the possible interactions between (pseudo-)protease subunits in the formation of the putative *AtFtsHi3* hexamer (based on our simplifying assumptions). **B,** Interaction diagrams of all possible binding partners in systems with 3 or 4 different subunits, organized by the frequency, in which we find non-monotonic behavior. Red circles indicate subunit A, the AtFtsHi3 pseudo-protease, and blue circles show other possible subunits B, C and D. Stars indicate the subunit with the most non-monotonic behavior. **C,** Bar graph showing the proportion of samples (mean of 10 samples of 100 simulations) that have monotonic behavior for subunit A (red) and non-monotonic behavior for other subunits (blue). The most isolated subunit (with star) is the one with most non-monotonic behavior. **D,** Concentrations of complexes containing different subunits (based on the interaction diagram C) are shown as a function of increasing expression of subunit A (FtsHi3). The arch in complexes containing subunit B drive the non-monotonic behavior.

in all other interactions. Non-monotonic behaviour is more commonly found in interactions where compound A could bind to more than one other subunit (in Figure S5, panels D-G should be compared to panels L-Q). In general, we observed that the models found in this paper were those, in which AtFtsHi3 could interact with at least two other protease subunits.

FtsH proteases are known to form homo- or heteromeric complexes (Sakamoto et al., 2003). To support our modelling data, the proteomic data were investigated for peptide abundance of other FtsH/FtsHis among the genotypes and treatments (Figure S6). Mitochondrial AtFtsH3 and/or AtFtsH10 were detectable in all comparisons except for the watered WT. Mitochondrial AtFtsH4 was only detected under drought conditions in the WT and *ftshi3-1* lines. The abundance of chloroplast thylakoid-located AtFtsH subunits did not vary across treatments or genetic lines, indicating that they are not strongly influenced by drought or the presence/absence of AtFtsHi3. However, specific FtsH proteases located in the chloroplast envelope (AtFtsH7, AtFtsH9, AtFtsH11, AtFtsH12, and AtFtsHi4) were only present in the *ftshi3-1* genotype under watered and drought conditions.

4 | DISCUSSION

4.1 | AtFtsHi3 overexpression results in a drought-tolerant phenotype

FtsHi pseudo-proteases are directly or indirectly involved in plant stress responses (Kadirjan-Kalbach et al., 2012; Lu et al., 2014; Kikuchi et al., 2018; Wang et al., 2018; Mishra et al., 2019; Mishra et al., 2021). While AtFtsHi1,2,4 and 5 are known to be subunits of a complex functioning in protein import into the chloroplast (Kikuchi et al., 2018; Schreier et al., 2018), the role of AtFtsHi3 remains unclear. Knock-down mutants of *ftshi3* (Kikuchi et al., 2018; Mishra et al., 2019; Mishra et al., 2021) tolerate abiotic stresses better than WT, the *ftshi3-1* knock-down mutant (*ftshi3-1*(kd), Mishra et al., 2021) was shown to be highly tolerant to drought. However, this plant line also displays growth reduction and a pale phenotype throughout its lifespan. Here, we describe and characterize AtFtsHi3 overexpression lines, which are drought tolerant but at the same time display enhanced growth and development (Figure 1, Figure S1). Although

the *AtFtsHi3* overexpression lines displayed similar or larger rosette sizes relative to the WT, they had a much higher survival rate after 15 days of drought (Table S1). Most rosettes of the overexpression lines were free of drought symptoms (Figure 3, Figure S2, Table S1), and their dry rosette biomass was significantly higher than in WT (Figure 3D). While overexpression lines under the native promoter might perform better due to the recognition and presence of the regulatory elements present in the endogenous promoter sequences (Hernandez-Garcia and Finer, 2014), we observed similar drought tolerance and even better growth during drought in lines regulated under the constitutive promotor (35SFtsHi3-OE) (Figure S2). The positive water-holding capacity of the overexpression lines under drought stress is likely a combination of several factors, including their reduced stomatal density and size (Figure S3B, C), leading to a higher WUE. These outcomes align with observations from the AtFtsHi3 knock-down mutant, demonstrating a pale-green dwarf phenotype and showcasing drought tolerance via a pathway independent of ABA (Mishra et al. 2021). Targeted knockout of the *GTL1* (GT-2 LIKE 1) transcription factor, which represses STOMATAL DENSITY AND DISTRIBUTION1 (*SDD1*), was shown to reduce stomatal density without affecting photosynthetic efficiency (Yoo et al., 2010). The *gtl1* mutants, as a result, possessed greater WUE, similar to the *ftshi3-1* mutant line (Mishra et al., 2021). In addition, a recent comparison of over 300 Arabidopsis cultivars demonstrated that reduced stomatal size increases WUE in Arabidopsis in general (Dittberner et al., 2018). The combination of a reduction in these two traits explains the increased WUE seen in our overexpression lines (Table S2).

While ABA concentrations were similar in *pFtsHi3-OE1* and *-OE2* lines compared to WT before the drought, they were not elevated to the same extent post-drought (Figure S3A). Since the accumulation of ABA induces guard cell closure (Daszkowska-Golec and Szarejko, 2013) and guard cell closure inherently improves WUE, reduced ABA levels (and thus open stomata) should result in decreased WUE. However, the opposite was observed in the *pFtsHi3-OE* and *35SFtsHi3-OE* lines (Table S2). These findings suggest that the *FtsHi3-OE* lines may have increased sensitivity to ABA or impaired their ability to sense drought. It is interesting to note that both proteomic (Table S6) and qPCR data (Table S3) indicate that the *ftshi3-1* mutant and *pFtsHi3-OE1* line consistently perceive a certain level of drought, although not to the extent of displaying drought symptoms. FtsHi3, therefore, could play a role in conveying the drought state of the plant.

4.2 | Pre-protein import related peptides accumulate in *ftshi3-1*

The *ftshi3* mutant displays a dwarf chlorotic phenotype, similar to the *hsp93/clpC1* mutants, which are known to cause pleiotropic effects and impair plant development and chloroplast biogenesis (Sjögren et al., 2004). These mutants also show increased levels of other CLP protease subunits (Sjögren et al., 2004). It is proposed that CLPC1 functions as a chaperone by acting as a translocation motor (Akita et al., 1997) that directly binds to TIC110, an essential component of the TIC translocation

complex responsible for importing chloroplast-targeted polypeptides (Kovacheva et al., 2005; Sjögren et al., 2014). Another chaperone protein, HSP90-III/CR88, which interacts with the TIC complex, is associated with reduced stature and delayed chloroplast development due to disrupted preprotein import (Cao et al., 2003). Notably, our proteomics data revealed elevated levels of HSP90, HSP93, and TIC110, as well as other TICs and TOCs (Figure S4). Considering the compensatory mechanism observed in *hsp93* mutants (Sjögren et al., 2004) and the similar phenotypes observed in *ftshi3-1*, *hsp90*, and *hsp93* mutants (Cao et al., 2003; Sjögren et al., 2004; Mishra et al., 2021), it could be possible that AtFtsHi3 plays a downstream role in pre-protein import into the thylakoid. This aligns with the growth-related phenotypes observed in the *ftshi3-1* mutant and *FtsHi3-OE* lines. However, further investigation, such as generating *ftshi3 hsp90* or *ftshi3 hsp93* double mutants, is required to validate this hypothesis.

AtFtsHi3 might impact, to some extent, the transmission of signals that promote growth (Kikuchi et al., 2018; Mishra et al., 2019, 2021). This is supported by the accumulation of proteins involved in isoprenoid metabolism, such as those for GGPP (geranylgeranyl pyrophosphate) and FPP (farnesyl pyrophosphate). GGPP is a precursor to several phytohormones, including gibberellins, strigolactones and abscisic acid (Lange and Ghassemian, 2003), whereas FPP is a substrate for the synthesis of a wide range of plant growth substances such as sterols, brassinosteroids and heme (Bouvier et al., 2005; Closa et al., 2010). The compensatory mechanisms for isoprenoids are unclear, but given that these proteins are absent in the WT: *pFtsHi3-OE* comparison, one can speculate that interrupted growth signalling may result in an accumulation of growth promoting precursors.

4.3 | The *ftshi3-1* and *pFtsHi3-OE* lines have overlapping changes in peptide abundance

In the present study rosettes from 6-week-old plants were investigated by shotgun proteomics to receive clues on the impact of AtFtsHi3 on plants´ drought tolerance and/or growth. Unfortunately, we were not able to identify the pseudo-protease in the proteome of pFtsHi3-OE1, despite high *AtFtsHi3* transcription under control conditions and even higher transcription during drought (Figure 3B). The reason why AtFtsHi3 has not been identified in this study or immunoprecipitation assays (Kikuchi et al., 2018) could be attributed to its rapid protein turnover. Alternatively, the AtFtsHi3-containing hexameric complex might be present only transiently in plants. In our previous studies, we observed AtFtsHi pseudo-proteases to be most important during the early stages of plant development (Mishra et al., 2019). To gain an understanding of AtFtsHi3 and its interacting partners, in future studies it might be beneficial to conduct proteomics studies on seedlings that are only 2 days old.

We were interested in identifying the common responses in the *ftshi3-1* mutant and *pFtsHi3-OE* lines to explore their resistance to drought (Figure 6). Under these growth conditions, several common proteins, including KIN1, AK4RC9, ABCG30, ABCG36, ABCG37, and LEA4-5, exhibited contrasting or distinct abundances in both *ftshi3-1*
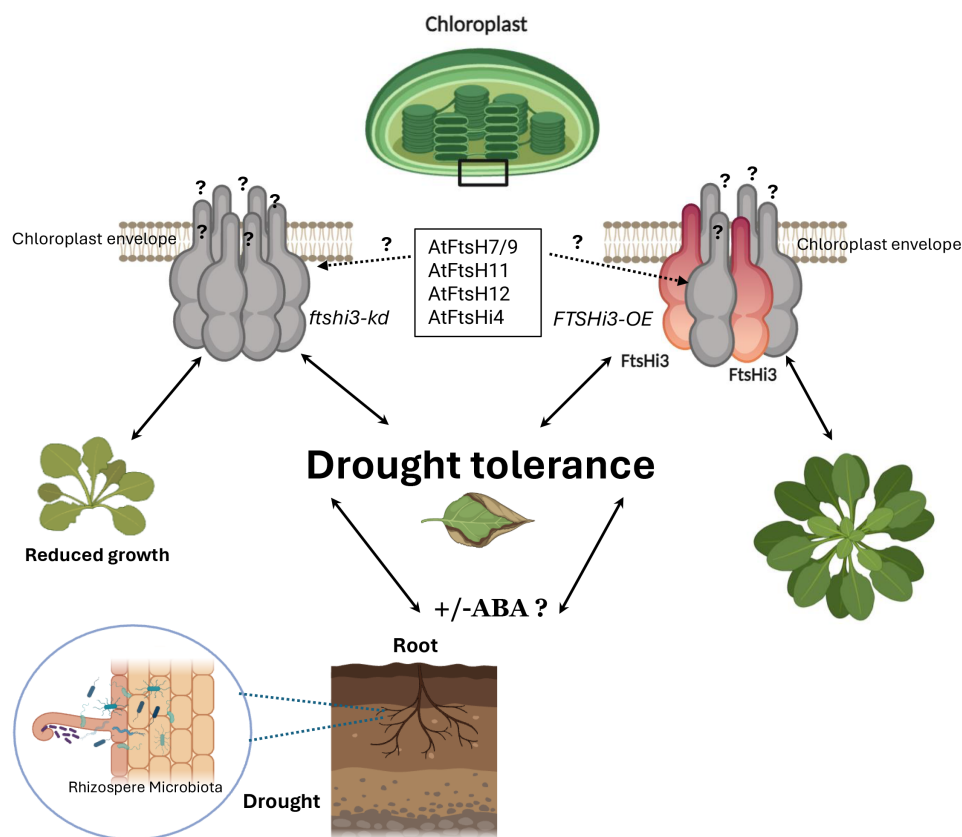
FIGURE 8 Schematic model about the impact of AtFtsHi3 on the plant phenotype in *Arabidopsis thaliana*. Absence of AtFtsHi3 in a hexamer leads to drought tolerance with reduced growth, while overexpression of the pseudo-protease also results in drought tolerance without affecting the growth. Possible partners in the hexamer might be AtFtsH7 or 9, AtFtsH11, AtFtsH12 or AtFtsHi4.

and *pFtsHi3-OE* lines compared to the WT. The ABCG proteins 30, 36, and 37 share a common identifying peptide, making it challenging to discuss their specific contributions to drought resistance. However, these proteins are elevated in *ftshi3-1* and *pFtsHi3-OE* lines while repressed in the WT under watered and droughted conditions, respectively. ABCG30 imports ABA to inhibit germination (Kang et al., 2015) and may also regulate root ABA transport. ABCG36, localized in the plasma membrane of roots and leaf epidermis (Strader and Bartel, 2009), transports indole-3-butyric acid and functions as an exclusion pump for sodium and cadmium, potentially enhancing drought resistance (Kim et al., 2007, 2010). ABCG36 transcript accumulation is not induced by drought or salt stress but is triggered by cadmium through WRKY13. ABCG37, expressed in the root epidermis, is involved in iron nutrition but likely has an insignificant contribution to drought resistance (Sheng et al., 2019). The elevated levels of ABCG36 in *pFtsHi3-OE* and *ftshi3-1* lines may partly explain their drought resistance. The elevation of corresponding transcripts remains unclear, although a WRKY13 protein was not detected in the proteomics data. One possibility is that their increased abundance is due to lower ABA levels in the OE lines, although *ftshi3-1* mutants reportedly maintain normal ABA levels during drought. Considering the diverse roles of these transporters in plant development and phytohormone regulation, the striking phenotype of *ftshi3-1* mutants can be understood. However, ABCG30's contribution to drought resistance is unlikely due to reduced ABA levels in *pFtsHi3-OE* and normal *ftshi3-1* lines.

LEA4-5 transcripts reach the highest levels in their family under stress conditions (Olvera-Carrillo et al. 2010). Despite similar transcript levels, there are some post-translational effects, as LEA4-5 protein abundance was higher in response to ABA than NaCl. Interestingly, data from our *ftshi3-1* and *pFtsHi3-OE* lines appears contrary to that of Olvera-Carrillo et al. (2010), since, in their analyses, reduced LEA4-5 transcription results in plants that have reduced biomass and fecundity and are drought sensitive. LEA4-5 overexpression lines are significantly drought-resistant. In our dataset, peptide abundance of LEA4-5 is reduced in the *ftshi3-1* and *pFtsHi3-OE* lines, but these plants retain their drought resistance. Since WT under drought accumulates the LEA4-5 peptide, as described by Olvera-Carrillo (2010), the reduced abundance in the *ftshi3-1* and *pFtsHi3-OE* lines may be some sort of compensatory response.

The molecular function of KIN1 is unclear, but as a well-documented drought- and ABA-responsive element (Wang et al., 1995), our proteomics data shows a curious trend. In the WT under both drought and watered conditions, KIN1 is similarly abundant, whereas both the *ftshi3-1* and *pFtsHi3-OE* lines have markedly reduced abundance, in line with the idea that these lines are not perceiving drought. However, since the levels of ABA are highly elevated in the droughted WT, the drought responsiveness of KIN1 in our experiment is not so clear.

The members of the ALDO-KETO REDUCTASE FAMILY 4 (AKR4C8-C11) play a crucial role in the metabolism of various sugars, steroids, and carbonyls. They can enhance various abiotic stress resistance by scavenging cytotoxic aldehydes in some plants (Yu et., al 2020).

Among these members, AKR4C8 is potentially involved in brassinosteroid metabolism (Simpson et al., 2009). Under stress conditions, both AKR4C8 and AKR4C9 transcripts show significant elevation (Simpson et al., 2009). In our dataset, AKR4C9 abundance is increased in both *ftshi3-1* and *pFtsHi3-OE* lines. In watered conditions, the WT exhibits reduced AKR4C9 abundance, while under drought, the enzyme's abundance is somewhat elevated, consistent with the drought-responsive nature of AKR4C9 transcripts (Simpson et al., 2009). Although the exact role it plays in conferring drought resistance remains unclear, AtFtsHi3 might have some implications for the downstream effect of AKR4C9.

4.4 | Particular binding patterns recapitulate the non-monotonic behaviour of putative AtFtsHi3-containing complexes

We used a mathematical approach to gain some insight into possible mechanisms that could give rise to our observations that the growth rate increases with increasing *AtFtsHi3* expression, yet stress tolerance shows non-monotonic behaviour (as long as expression of *AtFtsHi3* is different from WT, the mutant plants are drought-tolerant; Figure 7, Figure S5). The model was based on the data known for thylakoid-located AtFtsH proteases, which form a hetero-hexameric complex consisting of two types of FtsH subunits (FtsH1 and 5 are named type A; FtsH 2 and 8 named type B) (Sakamoto et al. 2003). Both types are required for active complexes, but AtFtsH1 and 5 can partly substitute for each other as can AtFtsH 2 and 8. A key aim of our modelling approach was to identify a minimal set of required features. We assumed the phenotype (either in terms of growth rate or stress tolerance) was determined by the proportion of specific pseudo-proteases within a population of interacting homo- or hetero-hexameric complexes. With this simple relationship, we found that complexes of at least three different interacting subunits could exhibit non-monotonic phenotypic behaviour. The frequency of non-monotonic behaviour increased in systems with four different interacting subunits, but it was not guaranteed. Indeed, our modelling results show that certain patterns of binding interactions are more likely to produce non-monotonic behaviour. For example, in systems of 4 different (pseudo-) protease subunits, non-monotonic behaviour is highest when AtFtsHi3 can bind to all other subunits. Moreover, in heteromeric complexes that show non-monotonic behaviour, a (pseudo-) protease subunit does not bind to at least one of the other subunits. Thus, our modelling predicts that AtFtsHi3 should be able to bind multiple partners and some of its partners should not be able to bind to each other. We note that such predictions are the product of many simplifying assumptions made in the absence of precise mechanistic information and are likely to change once more details are learned and included in the modelling. However, we conclude that non-monotonic phenotypic behaviour should be expected in many systems of heteromeric complexes and does not require much mechanical complexity. Based on our proteomic data, AtFtsH7 or 9, AtFtsH11, AtFtsH12 and/or AtFtsHi4 are possible partners to AtFtsHi3 (Figure S6) in a hexameric complex; they are upregulated in

ftshi3-1 independent of the growth condition and therefore might substitute for AtFtsHi3 in its absence.

5 | CONCLUSION

Although further investigations are needed, our study supports that AtFtsHi3 has implications for both growth and drought response. It is plausible to speculate that this pseudoprotease acts as a crucial switch that inhibits growth under unfavourable conditions (Figure 8). Due to its localization in the chloroplast envelope membrane, it is positioned in proximity to the TIC/TOC preprotein import system. Considering the abilities of other FtsHi proteins in translocating preproteins, it is reasonable to propose that AtFtsHi3 may also participate in this process (Kikuchi et al., 2018; Schreier et al., 2018). A transient AtFtsHi3 complex could be sufficient for acting on preprotein substrates, possibly explaining why it has not been detected in immunoprecipitation assays (Kikuchi et al., 2018) or in the *pFtsHi3-OE1* proteome.

We suggest the existence of a mechanism that relies on the stoichiometric balance of the AtFtsHi3 homo/heterohexamer complex. Similar protease complex systems have demonstrated changes in substrate preference with altered complex composition (Wojtkowiak et al., 1993). Under normal conditions, the hexamer exists in a state that allows effective communication of both growth and drought signals to the chloroplasts, thereby finely regulating photosynthesis and the trade-off between growth and drought resistance. In the *ftshi3-1* mutant, we observe a lack of perception of both growth and drought signals. However, in the overexpression lines, the complex exists in a state where substrate competition favours the transmission of putative growth signals, possibly at the expense of unidentified drought signals. It is also possible that this system functions in reverse, but further biochemical studies are necessary to explore this hypothesis.

DATA AVAILABILITY STATEMENT

ORCID

Christiane Funk [ID] https://orcid.org/0000-0002-7897-4038

REFERENCES

Akita M, Nielsen E, Keegstra K (1997) Identification of protein transport complexes in the chloroplastic envelope membranes via chemical cross-linking. *J Cell Biol* 136: 983–994.

Bittner LM, Arends J, Narberhaus F (2017) When, how and why? Regulated proteolysis by the essential FtsH protease in *Escherichia coli*. *Biol Chem* 398: 625–635.

Bouvier F, Rahier A, Camara B (2005) Biogenesis, molecular regulation and function of plant isoprenoids. *Prog Lipid Res* 44: 357–429.

Cao D, Froehlich JE, Zhang H, Cheng CL (2003) The chlorate-resistant and photomorphogenesis-defective mutant *cr88* encodes a chloroplast-targeted HSP90. *Plant J* 33: 107–118.

Closa M, Vranová E, Bortolotti C, Bigler L, Arró M, Ferrer A, Gruissem W (2010) The *Arabidopsis thaliana* FPP synthase isozymes have overlapping and specific functions in isoprenoid biosynthesis, and complete loss of FPP synthase activity causes early developmental arrest. *Plant J* 63: 512–525.

Clough SJ, Bent AF (1998) Floral dip: A simplified method for *Agrobacterium*-mediated transformation of *Arabidopsis thaliana*. *Plant J* 16: 735–743.

Cox J, Neuhauser N, Michalski A, Scheltema RA, Olsen J V., Mann M (2011) Andromeda: A peptide search engine integrated into the MaxQuant environment. *J Proteome Res* 10: 1794–1805.

Czechowski T, Stitt M, Altmann T, Udvardi MK, Scheible WR (2005) Genome-wide identification and testing of superior reference genes for transcript normalization in Arabidopsis. *Plant Physiol* 139: 5–17.

Daszkowska-Golec A, Szarejko I (2013) Open or close the gate - Stomata action under the control of phytohormones in drought stress conditions. *Front Plant Sci* 4: 1–16.

Dittberner H, Korte A, Mettler-Altmann T, Weber APM, Monroe G, De Meaux J (2018) Natural variation in stomata size contributes to the local adaptation of water-use efficiency in *Arabidopsis thaliana*. *Mol Ecol* 27: 4052–4065.

Fanourakis D, Nikoloudakis N, Pappi P, Markakis E, Doupis G, Charova SN, Delis C, Tsaniklidis G (2020) The role of proteases in determining stomatal development and tuning pore aperture: A review. *Plants* 9: 1–11.

Haas JC, Vergara A, Serrano AR, Mishra S, Hurry V, Street NR (2021) Candidate regulators and target genes of drought stress in needles and roots of Norway spruce. *Tree Physiol* 41: 1230–1246.

Harb A, Pereira A (2011) Screening Arabidopsis Genotypes for Drought Stress Resistance. In *Plant Reverse Genetics*: 191–198. Humana Press, Totowa, NJ.

Hellens R, Mullineaux P, Klee H (2000) A guide to *Agrobacterium* binary Ti vectors. *Trends Plant Sci* 5: 446–451.

Hernandez-Garcia CM, Finer JJ (2014) Identification and validation of promoters and *cis*-acting regulatory elements. *Plant Sci* 217–218: 109–119.

Kadirjan-Kalbach DK, Yoder DW, Ruckle ME, Larkin RM, Osteryoung KW (2012) *FtsHi1/ARC1* is an essential gene in Arabidopsis that links chloroplast biogenesis and division. *Plant J* 72: 856–867.

Kang J, Yim S, Choi H, Kim A, Lee KP, Lopez-Molina L, Martinoia E, Lee Y (2015) Abscisic acid transporters cooperate to control seed germination. *Nat Commun*. doi: https://doi.org/10.1038/ncomms9113

Kikuchi S, Asakura Y, Imai M, Nakahira Y, Kotani Y, Hashiguchi Y, Nakai Y, Takafuji K, Bédard J, Hirabayashi-Ishioka Y, et al (2018) A Ycf2-FtsHi heteromeric AAA-ATPase complex is required for chloroplast protein import. *Plant Cell* 30: 2677–2703.

Kim DY, Bovet L, Maeshima M, Martinoia E, Lee Y (2007) The ABC transporter AtPDR8 is a cadmium extrusion pump conferring heavy metal resistance. *Plant J* 50: 207–218.

Kim DY, Jin JY, Alejandro S, Martinoia E, Lee Y (2010) Overexpression of AtABCG36 improves drought and salt stress resistance in Arabidopsis. *Physiol Plant* 139: 170–180.

Knudsen S (1999) Promoter2.0: For the recognition of PolII promoter sequences. *Bioinformatics* 15: 356–361.

Kovacheva S, Bédard J, Patel R, Dudley P, Twell D, Ríos G, Koncz C, Jarvis P (2005) In vivo studies on the roles of Tic110, Tic40 and Hsp93 during chloroplast protein import. *Plant J* 41: 412–428.

Lange BM, Ghassemian M (2003) Genome organization in *Arabidopsis thaliana*: A survey for genes involved in isoprenoid and chlorophyll metabolism. *Plant Mol Biol* 51: 925–948.

Libby E, Lind P (2019) Probabilistic models for predicting mutational routes to new adaptive phenotypes. *BIO-PROTOCOL*, 9(20). https://doi.org/10.21769/bioprotoc.3407

Lu X, Zhang D, Li S, Su Y, Liang Q, Meng H, Shen S, Fan Y, Liu C, Zhan C (2014) FtsHi4 Is Essential for Embryogenesis Due to Its Influence on Chloroplast Development in *Arabidopsis*. *PLoS One* 15: e0229232.

Martin J (2021) Regulation | AAA-ATPases. *Encycl. Biol. Chem. III* (Third Ed. pp 513–523).

Mishra LS, Mielke K, Wagner R, Funk C (2019) Reduced expression of the proteolytically inactive FtsH members has impacts on the Darwinian fitness of *Arabidopsis thaliana*. *J Exp Bot* 70: 2173–2184.

Mishra LS, Mishra S, Caddell DF, Coleman-Derr D, Funk C (2021) The Plastid-Localized AtFtsHi3 Pseudo-Protease of *Arabidopsis thaliana* Has an Impact on Plant Growth and Drought Tolerance. *Front Plant Sci*. doi: https://doi.org/10.3389/fpls.2021.694727

Moldavski O, Levin-Kravets O, Ziv T, Adam Z, Prag G (2012) The heterohexameric nature of a chloroplast AAA+ FtsH protease contributes to its thermodynamic stability. *PLoS One*. doi: https://doi.org/10.1371/journal.pone.0036008

Murashige T, Skoog F (1962) A revised medium for rapid growth and bioassays with tobacco tissue cultures. *Physiol plant* 15: 473–497.

Nauta K, Miller RE (2000) Formation of cyclic water hexamer in liquid helium: The smallest piece of ice. *Science (80-)* 287: 293–295.

Nishimura K, Kato Y, Sakamoto W (2016) Chloroplast proteases: Updates on proteolysis within and across suborganellar compartments. *Plant Physiol* 171: 2280–2293.

De Ollas C, Segarra-Medina C, González-Guzmán M, Puertolas J, Gómez-Cadenas A (2019) A customizable method to characterize *Arabidopsis thaliana* transpiration under drought conditions. *Plant Methods* 15: 1–15.

Olvera-Carrillo Y, Campos F, Reyes JL, Garciarrubio A, Covarrubias AA (2010) Functional analysis of the group 4 late embryogenesis abundant proteins reveals their relevance in the adaptive response during water deficit in Arabidopsis. *Plant Physiol* 154: 373–390.

Prokhorova TA, Blow JJ (2000) Sequential MCM/P1 subcomplex assembly is required to form a heterohexamer with replication licensing activity. *J Biol Chem* 275: 2491–2498.

Ramundo S, Asakura Y, Salomé PA, Strenkert D, Boone M, Mackinder Lcm, Takafuji K, Dinc E, Rahire M, Crèvecoeur M, et al (2020) Coexpressed subunits of dual genetic origin define a conserved supercomplex mediating essential protein import into chloroplasts. *Proc Natl Acad Sci U S A* 117: 32739–32749.

Sakamoto W, Zaltsman A, Adam Z, Takahashi Y (2003) Coordinated Regulation and Complex Formation of YELLOW VARIEGATED1 and

YELLOW VARIEGATED2, Chloroplastic FtsH Metalloproteases Involved in the Repair Cycle of Photosystem II in Arabidopsis Thylakoid Membranes. *Plant Cell* 15: 2843–2855.

Schreier TB, Cléry A, Schläfli M, Galbier F, Stadler M, Demarsy E, Albertini D, Maier BA, Kessler F, Hörtensteiner S, et al (2018) Plastidial NAD-dependent malate dehydrogenase: A moonlighting protein involved in early chloroplast development through its interaction with an ftsh12-ftshi protease complex. *Plant Cell* 30: 1745–1769.

Seleiman MF, AL-Suhaibani N, Ali N, Akmal M, Alotaibi M, Refay Y, Dindaroglu T, Abdul-Wajid HH, Battaglia ML (2021) Drought stress impacts on plants and different approaches to alleviate its adverse effects. *Plants* 10: 1–25.

Sheng Y, Yan X, Huang Y, Han Y, Zhang C, Ren Y, Fan T, Xiao F, Liu Y, Cao S (2019) The WRKY transcription factor, *WRKY13*, activates *PDR8* expression to positively regulate cadmium tolerance in Arabidopsis. *Plant Cell Environ* 42: 891–903.

Simpson PJ, Tantitadapitak C, Reed AM, Mather OC, Bunce CM, White SA, Ride JP (2009) Characterization of Two Novel Aldo-Keto Reductases from Arabidopsis: Expression Patterns, Broad Substrate Specificity, and an Open Active-Site Structure Suggest a Role in Toxicant Metabolism Following Stress. *J Mol Biol* 392: 465–480.

Sjögren LLE, Macdonald TM, Sutinen S, Clarke AK (2004) Inactivation of the *clpC1* gene encoding a chloroplast Hsp100 molecular chaperone causes growth retardation, leaf chlorosis, lower photosynthetic activity, and a specific reduction in photosystem content. *Plant Physiol* 136: 4114–4126.

Sjögren LLE, Tanabe N, Lymperopoulos P, Khan NZ, Rodermel SR, Aronsson H, Clarke AK (2014) Quantitative analysis of the chloroplast molecular chaperone ClpC/Hsp93 in Arabidopsis reveals new insights into its localization, interaction with the Clp proteolytic core, and functional importance. *J Biol Chem* 289: 11318–11330.

Smakowska E, Czarna M, Janska H (2014) Mitochondrial ATP-dependent proteases in protection against accumulation of carbonylated proteins. *Mitochondrion* 19: 245–251.

Sokolenko A, Pojidaeva E, Zinchenko V, Panichkin V, Glaser VM, Herrmann RG, Shestakov S V. (2002) The gene complement for proteolysis in the cyanobacterium Synechocystis sp. PCC 6803 and *Arabidopsis thaliana* chlorophlasts. *Curr Genet* 41: 291–310.

Strader LC, Bartel B (2009) The Arabidopsis PLEIOTROPIC DRUG RESISTANCE8/ABCG36 ATP binding cassette transporter modulates sensitivity to the auxin precursor Indole-3-butyric acid. *Plant Cell* 21: 1992–2007.

Tomeo NJ, Rosenthal DM (2018) Photorespiration differs among *Arabidopsis thaliana* ecotypes and is correlated with photosynthesis. *J Exp Bot* 69: 5191–5204.

Tyanova S, Temu T, Cox J (2016) The MaxQuant computational platform for mass spectrometry-based shotgun proteomics. *Nat Protoc* 11: 2301–2319.

Vaseva I, Akiscan Y, Demirevska K, Anders I, Feller U (2011) Drought stress tolerance of red and white clover-comparative analysis of some chaperonins and dehydrins. *Sci Hortic (Amsterdam)* 130: 653–659.

Wagner R, Aigner H, Funk C (2012) FtsH proteases located in the plant chloroplast. *Physiol Plant* 145: 203–214.

Wang H, Datla R, Georges F, Loewen M, Cutler AJ (1995) Promoters from *kin1* and *cor6.6*, two homologous *Arabidopsis thaliana* genes: transcriptional regulation and gene expression induced by low temperature, ABA, osmoticum and dehydration. *Plant Mol Biol* 28: 605–617.

Wang T, Li S, Chen D, Xi Y, Xu X, Ye N, Zhang J, Peng X, Zhu G (2018) Impairment of FtsHi5 Function Affects Cellular Redox Balance and Photorespiratory Metabolism in Arabidopsis. *Plant Cell Physiol* 59: 2526–2535.

Wojtkowiak D, Georgopoulos C, Zylicz M (1993) Isolation and characterization of ClpX, a new ATP-dependent specificity component of the Clp protease of *Escherichia coli*. *J Biol Chem* 268: 22609–22617.

Yoo CY, Pence HE, Jin JB, Miura K, Gosney MJ, Hasegawa PM, Mickelbart M V. (2010) The Arabidopsis GTL1 transcription factor regulates water use efficiency and drought tolerance by modulating stomatal density via transrepression of SDD1. *Plant Cell* 22: 4128–4141.

Yu J, Sun H, Zhang J, Hou Y, Zhang T, Kang J, Wang Z, Yang Q, Long R. (2020) Analysis of Aldo-Keto Reductase Gene Family and Their Responses to Salt, Drought, and Abscisic Acid Stresses in *Medicago truncatula*. *Int J Mol Sci*. Jan 23;21(3): 754. doi: https://doi.org/10.3390/ijms21030754.

SUPPORTING INFORMATION

Additional supporting information can be found online in the Supporting Information section at the end of this article.